Enhanced multiplex binary PIR localization using the Transferable Belief Model

A. Henni, R Ben Bachouch, Ouafae Bennis, Nacim Ramdani

Enhanced multiplex binary PIR localization using the Transferable Belief Model

A. HADJ HENNI, R. BEN BACHOUCH, O. BENNIS and N. RAMDANI

***Abstract*—Pyro-electric Infra Red (PIR) sensors have been widely used in different indoor localization applications during the last decade. These sensors are cheap, non-intrusive and non-wearable, nevertheless, the binary PIR sensor detects only the presence of a human motion in its field of view without any other information about the actual location. Therefore, to localize a person in different zones of interest, the use of several PIR sensors with overlapping field of view is necessary. To reduce the number of sensors used, we use multiplex masks with the binary PIR sensors to obtain a compressed overlapping structure. Such a structure induces ambiguity during transitions between zones. In this paper, we show how to circumvent this issue by using a novel localization algorithm based on the transferable belief model TBM. Besides, we show how to tune efficiently the parameters of our algorithm, by choosing an appropriate discounting factor within (TBM). Experiments using standard commercialized sensors equipped with the multiplex masks, emphasize the performance of our novel method**

***Index Terms*—Indoor localization, binary PIR sensing, transferable belief model, sensors data fusion, smart homes.**

I. Introduction

NOWADAYS, the human indoor location-tracking using sensor networks has become a necessity for several smart home applications such as anti-intrusion security systems, comfort and energy optimization, and elderly monitoring. A large range of indoor localization systems has been investigated during the last decade, and different sensing technologies were used depending on the considered smart home application. These systems can be mainly divided into two types, the wearable and the non-wearable device systems as shown in a recent survey [1].

In this paper, we are interested in an elderly monitoring application which rather requires non-wearable devices since they are more convenient and more comfortable for the elderly. Among the non-wearable devices, the Pyro Infra-Red PIR sensors are often used alone or with other sensing modalities in smart home applications. In fact, *E.Ahvar et al* [1] have analyzed some non-wearable localization systems w.r.t their technical and technological features, and discussed their advantages and inconveniences Relying on this analysis, we note that cheap and reliable non-wearable systems often involve PIR sensors. The latter are inexpensive compared to other technologies, are non-intrusive and have low energy consumption. A PIR sensor detects thermal variations occurring in its FOV (Field of View) and translates the variations as an electrical signal known as analog output. The latter can be processed either to provide information such as angle and direction of movement, speed and distance from sensor [2] [3], or for zoning the moving target as in [4]. Nevertheless, analog outputs are not widely used for indoor location-tracking applications due to the processing time and the intensive computing resources they require, and also to the saturation of the communication network they induce. Therefore, the analog output is often converted into a binary output to provide only binary data such as presence/absence of a human motion. Related works that use binary PIR outputs for indoor localization can be divided into two categories depending on the sensor network structure.

The first category uses PIR sensor networks without overlapping FOV *e.g.* each room is covered only by one sensor as in [5]. However, in some elderly monitoring applications, several activities can be done within the same room which requires covering each zone of interest with its own sensor to discern the different activities within a same room as in [6]. Unfortunately, covering each zone with its own PIR sensor is not always easy due to sensor placement constraints as induced by the presence of different obstacles [7] or constraints related to the smart home architecture. For instance, when several activity zones (*i.e.* zones of interest) are close to each other within the room, the FOV of the sensors of two neighboring zones may overlap other zone(s) of interest, hence, the FOV's overlapping structure cannot be avoided.

The second category of systems uses binary PIR sensor networks with overlapping FOVs. Such structure suffers from invalid intersections caused by the interference between different PIR FOVs even when tracking a single target. To cope with this issue, *Bo.Yang et al* proposed several methods in recent years either using classifiers, which require a training phase as in [8], or without classifiers as in [9]. These methods use specific sensor-nodes with 6 PIRs per node, however, such sensor nodes may increase the data throughput due to the important number of sensors used. Also, designing such sensor nodes is not always easy in practice since it requires deep technical skills and technological knowledge. Moreover, *Bo.yang et al* works deal with target position coordinates as in [10]. To reduce the number of PIR sensors used in an indoor localization application, a compressive binary PIR structure was proposed in [11][12] by adding so-called multiplex masks to the PIR sensors. Nevertheless, the application in these studies [11][12] relies on some geometric information in order to enhance the location resolution which is similar to the case of study in [13]. In our case, we are not interested in the precise coordinates of the user's position nor in enhancing the location resolution, we rather aim at estimating the probability of presence over some predefined zones of interest.

This work was funded by the french CoCaPs project issued from FUI 20. All authors are with the Univ. Orleans, INSA-CVL, PRISME, EA 4229, F45072, Orleans, France. Corresponding author: A. HADJ HENNI (raouf.hadj.henni@gmail.com)

Our application falls within the same work as in [6] which addresses human indoor localization within zones of interest using binary PIR sensors for a telehomecare application, that is the monitoring of a person living alone. The localization algorithm in [6] relies on Bayesian filtering, using a probabilistic motion model and past location estimates for prediction, while the likelihoods are specified manually for each zone by the person in charge of the configuration. The main drawback of the method used in [6] resides in the large number of sensors required to cover the zones of interest, since each zone was covered by its own specific sensor. Also, allowing a person specifying a list of boolean expressions for each zone to obtain likelihoods depending on activated sensor(s) is a tedious task, even more when the number of zones is large. To cope with this drawback, we have recently extended this localization approach, first by using a multiplex overlapping structure to reduce the number of needed sensors when covering the zones of interest, and second by automatically computing the likelihoods without using boolean expressions [14].

Nevertheless, only simulation results were presented as evaluation of the Bayesian filtering in [14] as it appeared that the overlapping structure of our system induces ambiguity when the person transits between zones. This is because during a transition, the sensors of both neighboring zones may activate leading to the erroneous signature of an other neighboring zone. Such transition issue has already been identified in [6] as the main source explaining large location errors.

In this paper, the first contribution addresses the ambiguity issue induced by the transitions between zones, by using an alternative framework. We propose a prediction-correction filtering algorithm based on the Transferable Belief Model (TBM) framework [15] instead of the Bayesian framework since TBM can naturally handle such ambiguity through the power set. The localization is performed by combining two different information sources namely the prediction, which is obtained using past location results and a human motion model, and the observation source which updates the prediction relying on the sensor network measurement data. The trade-off between the two sources depends on whether a transition between zones is occurring or not, a situation that can be distinguished relying on the received measurement data.

The second contribution of this paper addresses an efficient tuning of TBM. We propose a novel way for choosing an appropriate discounting factor, which is a factor used to weight an information source compared to other source(s) within TBM. The appropriate value is chosen by analyzing the behavior of the Dempster-Shafer (DS) normalization function in order to avoid counter-intuitive location results after DS normalization.

Finally, experiments using commercialized sensors, for which we modify the field of view using multiplex masks, show the performance of our novel algorithm compared to the one we presented in [14]. The rest of this paper is organized as follows: Section II presents some aspects of the TBM framework. Section III describes the sensors specifications and their deployment. Section IV describes our novel localization approach using the TBM. Section V shows the experimental results and section VI concludes the paper.

II. Aspects of the Transferable Belief Model

This section presents some TBM theoretical aspects which are used next in our localization algorithm.

A. Main definitions:

TBM is a theoretical framework that uses belief functions to represent knowledge about given hypotheses, but also about sets of these hypotheses. It can be considered as an alternative to Dempster-Shafer theory DST [16] with some extensions and additional tools. Among the common aspects between TBM and DST, we have the mass function denoted m and the power set 2^Ω. Let the set of hypotheses $\Omega = \{h_1, h_2, ..h_n\}$ be the Frame of Discernment (FoD), and let $2^\Omega = \{\{\phi\}, \{h_1\}, ..., \{h_1, h_2\}, ..., \{\Omega\}\}$ be the power set of Ω. A mass function $m(H)$ over a hypothesis (*i.e.* when $H = h_i$) or over a set of hypotheses (*i.e.* when $H = \{h_i, .., h_j\}$), takes values in the range [0, 1]. It is assigned to all elements H of the power set 2^Ω and satisfies:

$$\sum_{H \in 2^\Omega} m(H) = 1.$$

The elements H of 2^Ω that may have $m(H) > 0$ are called *focal elements*. The set of all focal elements is denoted ξ. The power set 2^Ω allows us to represent the knowledge over a set of hypotheses which represents the uncertainty when we are not sure about a singleton (*i.e. a single element* of Ω). This is the main advantage compared to frameworks based on the probability theory such as the Bayes framework. Other common aspects between TBM and DST are the belief function $Bel(.)$ and the plausibility function $Pl(.)$ defined for all $H_k \subseteq \Omega$ as:

$$Bel(H_k) = \sum_{H_i | H_i \subseteq H_k} m(H_i),$$

$$Pl(H_k) = \sum_{H_i | H_i \cap H_k \neq \phi} m(H_i).$$

The belief $Bel(H_k)$ (*resp* the plausibility $Pl(H_k)$) represents the lower bound (*resp* the upper bound) of the probability of H_k *i.e.*

$$Bel(H_k) \leq Prob(H_k) \leq Pl(H_k).$$

B. Basic combination rules:

Several combination rules exist within the TBM framework, among them, there is the conjunctive rule and its normalized version which corresponds to the DS rule, and the disjunctive rule *known as* the prudent rule. Let $A, \in 2^\Omega$, and let m_1, m_2 be mass functions obtained from two independent knowledge sources. The conjunctive rule is then:

$$\forall A \in 2^\Omega,\ m_{1\cap 2}(A) = \sum_{B,C \in 2^\Omega, B \cap C = A} m_1(C) \cdot m_2(B). \quad (1)$$

Then, the normalized conjunctive rule, *i.e.* DS rule is:

$$\forall A \in 2^\Omega \setminus \phi,\ m_{1\oplus 2}(A) = \frac{1}{1 - m_{1\cap 2}(\phi)} \cdot m_{1\cap 2}(A), \quad (2)$$

and $m_{1\oplus 2}(\phi) = 0$. Finally, the disjunctive combination rule is:

$$m_{1\cup 2}(A) = m_1 \cup m_2(A) = \sum_{B\cup C = A \neq \phi} m_1(C) \cdot m_2(B). \quad (3)$$

Note that all these combination rules require that both mass functions are defined over the same frame of discernment and their sources must be independent sources of evidence.

C. Operations over FODs:

This subsection presents only some operations over FoDs which are used in this paper.

1) Refinement and vacuous extension: Let Ω be a frame of discernment and Ω' be a refinement of Ω, *i.e.*, each hypothesis h_i of Ω has an image in one or in a set of hypotheses of Ω'. This means that hypotheses of Ω are more detailed in Ω' by splitting at least one hypothesis h_i of Ω into several hypotheses in Ω'. Refinement operations over FoDs can be generalized to mass functions.

Let m^Ω be a mass function over Ω, and let $\rho()$ be the refinement function *i.e.* $\Omega' = \rho(\Omega)$. The mass m^Ω can be transferred to Ω' through the *vacuous extension* $m^{\Omega\uparrow\Omega'}$ as follows:

$$m^{\Omega\uparrow\Omega'}(h') = \begin{cases} m^\Omega(h) & \text{if} \quad h' = \rho(h) \\ 0 & \text{otherwise} \end{cases} \quad (4)$$

with $h \in \Omega$ and $h' \in \Omega'$.

2) Coarsening: Coarsening, the dual operation of refinement, reduces the size of a FoD by making it more coarse, *i.e.* if Ω' is a refinement of Ω ($\Omega' = \rho(\Omega)$) then Ω is a coarsening of Ω'. Nevertheless, the refinement is not always surjective *i.e.* some element(s) of $2^{\Omega'}$ may not have image(s) on 2^Ω. This issue leads to *inner* and *outer* reduction as pointed in DST [16, pp 117-118].

3) Inner and outer reduction: Inner reduction $\underline{\omega}$ and outer reduction $\overline{\omega}$ are functions from 2^Ω to $2^{\Omega'}$ that satisfy:

$$\underline{\omega}(A) = \{\omega \in \Omega \,|\, \rho(\{\omega\}) \subseteq A\} \quad (5)$$

$$\overline{\omega}(A) = \{\omega \in \Omega \,|\, \rho(\{\omega\}) \cap A \neq \phi\} \quad (6)$$

where $A \subseteq \Omega'$ and $\Omega' = \rho(\Omega)$.

The inner (*resp* outer) reduction concept can be extended to mass functions as in (7) (*resp* in (8)) :

$$\underline{m}^\Omega(\omega) = \sum_{A\subseteq\Omega', \underline{\omega}(A)=\omega} m^{\Omega'}(A), \quad \forall \omega \subseteq \Omega \quad (7)$$

$$\overline{m}^\Omega(\omega) = \sum_{A\subseteq\Omega', \overline{\omega}(A)=\omega} m^{\Omega'}(A), \quad \forall \omega \subseteq \Omega \quad (8)$$

More details and examples about *inner* and *outer* reduction can be found in [17]

D. Pignistic transform

Within TBM, the pignistic probability $BetP$ can be used to transform the mass function m^Ω of a singleton into a probability by transferring the mass functions of an uncertainties as follows:

$$BetP^\Omega(C) = \frac{1}{1 - m^\Omega(\phi)} \sum_{A\subseteq\Omega,\, c\in A} \frac{m^\Omega(A)}{\mid A \mid} \quad (9)$$

where $\mid A \mid$ is the cardinal of A *i.e.* is the number of elements in A.

III. Sensors details and deployment

A. PIR sensors details

In our application, we use wall-mounted 180° PIR sensors commercialized* by *Legrand* company and shown in *Fig.2.a* Each sensor is provided along with the mask shown in *Fig.2.b* that can be used to cover one or several angles of view.

The provided mask is easy to cut with pliers, nevertheless, large errors on the FoV were obtained during experimental tests since the mask is not deep enough. For instance, if we cut a portion of 30° we will obtain a FoV of around 50° or more instead of 30°. To minimize such large error and obtain consistent angles w.r.t desired FoVs, we add a 3D printed shields *Fig.2.c* and paste them with the provided mask using standard glue gun to obtain our own multiplex masks as shown in *Fig.2.d*. Such a manipulation does not require deep technological knowledge nor high technical skills compared to the manipulations required for designing the specific sensor nodes as in [8] . Note that the shields used are effective, however, other shields can be investigated.

Since a PIR sensor detects human motions based on a thermal variation, it is also sensitive to any other thermal variation caused by non-human objects (*e.g.* heater, airflow, ..etc.) which may induce erroneous measurement known as *false positive*. In addition, such sensors may miss some human motions depending on the distance from the sensor and on the motion's nature (large/small motion, radial/tangential motion w.r.t the sensor, ..etc.) which leads to *false negative*.

The sensors outputs are sent through a KNX communication network and are acquired using its associated ETS software[1].

B. The living lab and sensors deployment

Fig.1.a) illustrates the living lab GIS MADONAH[2] which is a nursing home equipped with different sensors and technologies to study senior's behavior in order to improve his/her home support and nursing. For this purpose, and for subsequent decision making studies, we need to localize the person within some predefined zones of interest. The zoning of the living lab is shown in *Fig.1.b)* and obtained using seven PIR sensors along with multiplex masks with different FOVs. Each sensor has two FOVs except for *purple* and *green* sensors[3], and the uncovered FOVs are marked with discontinuous arcs. The living lab is divided then into thirteen different zones but note that some of these zones are not linked to activities (*e.g.* $Zone3.a, Zone3.b$ and $Zone6$). Such zones are obtained due to the overlapping structure and can be considered as *passage* zones instead of activity zones. Also, very small zones are not considered due to their small size (*e.g.* zone between $Zone6$ and $Zone9$) since if the person moves inside them he/she will activate sensors of their large neighboring zones, hence,

*http://www.legrandoc.com/048920

[1]http://www.knx.fr/KNX-France-ets5.html

[2]http://www.bourges.univ-orleans.fr/madonah/index.php/experimentations

[3]Colors are used in order to easily distinguish the different sensors and the code of each zone.

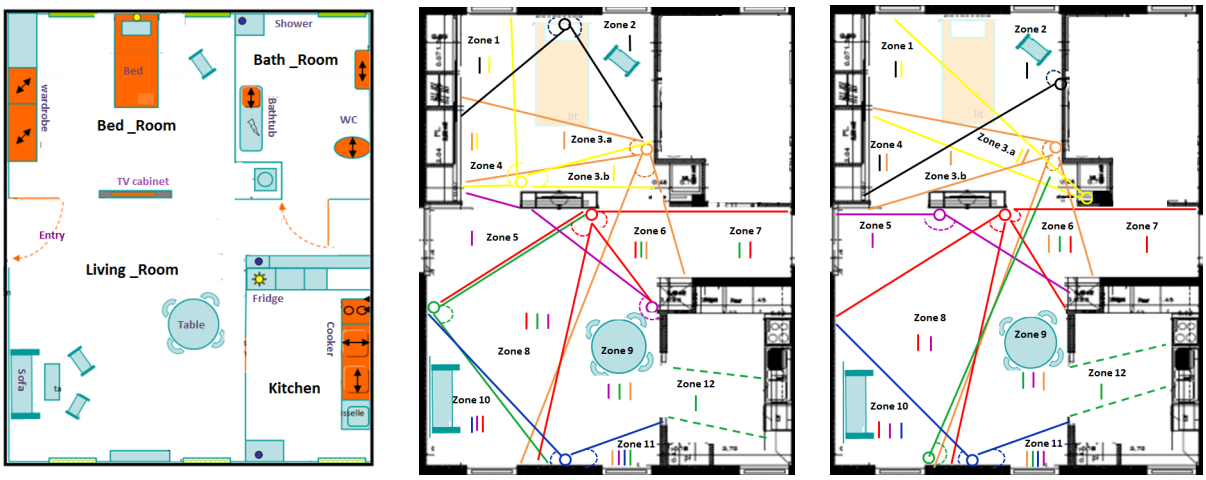

(a) Map of the living lab (b) Living lab zoning with *deployment A* (c) Living lab zoning with *deployment B*

Fig. 1: Living lab description and zoning. Uncovered FOVs are marked with discontinuous arcs in (b) and (c).

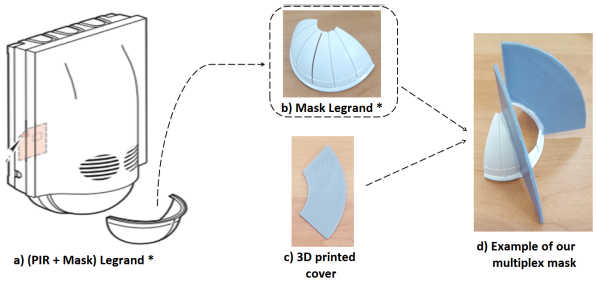

Fig. 2: Example of a 180° PIR sensor used in our case.

they correspond rather to transitions. The $BathRoom$ is not considered and the kitchen is partially considered in this paper. The bed zone is not considered since a bed rest sensor will be used subsequently.

To further investigate the impact of sensors deployment on our novel localization method, we have considered another deployment $Deployment\ B$ (where $Green$, $Purple$, $Yellow$, and $Black$ sensors have been moved to other walls) as shown in Fig.1.c). Remember that we are interested in covering some specific zones of interest, hence, the $Deployment\ B$ should cover more or less the same zones as $Deployment\ A$.

C. Zone validation:

The validation of each zone is obtained by performing several large motions inside the considered zone and by checking the activation of the sensors covering it. For example, to validate $Zone10$ we performed several walking motions within and around the sofa and checked that the $Blue$, Red and $Purple$ sensors will activate. Note that a reasonable uncertainty on the sensor's FOV is not really problematic as long as the zones of interest are still covered by the desired sensors. Indeed, since we are more interested next in the activities and not in the exact position coordinates, we just need to make sure that the person is inside the activity zone regardless of its size variation (*e.g.* ensure that the person is on the sofa regardless the shape of $Zone10$), consequently, the FOV's variations are related rather to transitions.

Each of the thirteen zones has a color code corresponding to the sensor(s) covering it. With such a zoning, it is clear that *false positive* and *false negative* are critical issues. For example, if the person is moving inside $Zone12$ and if the red sensor is activated due to a *false positive*, we will receive a measurement (red + green activated) corresponding to $Zone7$ in Fig.1.b). To the contrary, if the person is moving inside $Zone7$ and red sensor will not detect the motion due to a *false negative* (caused by a radial motion w.r.t red sensor) we will receive green alone as a measurement which corresponds to $Zone12$. Such *false positive* and *false negative* can be overcome through filtering (*i.e.* prediction/correction) techniques such as in our previous approach [14]. Nevertheless, the latter method cannot overcome the ambiguity issues induced by the transitions such as the one between $Zone3.b$ and $Zone3.a$ which sensors activation signature is the same as the signature of $Zone4$ in Fig.1.b. This may easily lead to localization errors if we do not handle the transitions between zones.

IV. Our Novel Localization Approach

A. Problem formulation

The localization problem is formulated as a state estimation problem and solved using a prediction-correction filtering algorithm. Prediction is obtained using the past location estimates and a human motion model. Correction exploits the binary outputs provided by the PIR sensor networks. Since we will combine the prediction with the measurements data within TBM, the first step is to define the Frame of Discernment (FoD) of each source.

Let Ω_{pre} (*resp* Ω_{obs}) be the prediction's FoD (*resp* the observation's FoD). These two FoDs are defined for each $Zone(i)$ as follows:

$$\Omega_{pre} = \{Inside, \overline{Inside}\}, \quad (10)$$

$$\Omega_{obs} = \{Inside, Neigh, Far\}. \quad (11)$$

where $Neigh \cup Far = \overline{Inside}$. The power sets are

$$2^{\Omega_{pre}} = \{\phi, Inside, \overline{Inside}, \Omega_{pre}\}, \quad (12)$$

$$2^{\Omega_{obs}} = \{\phi, Inside, Neigh, Far, \underbrace{Inside \cup Neigh}_{Transition}, Inside \cup Far, \underbrace{Neigh \cup Far}_{\overline{Inside}}, \Omega_{obs}\}. \quad (13)$$

Therefore, it is clear that Ω_{obs} is a refinement of Ω_{pre}.

Ω_{pre} contains two hypotheses which state that a person is either inside or outside a considered $Zone(i)$. In fact, for each $Zone(i)$ we only predict if the person will be inside or outside the zone, because of the motion model used as detailed further in Sect.IV-B. However, Ω_{obs} contains more details since by considering the sensor network data instead of a single sensor data we can distinguish when the person is inside the zone, transiting to a neighbor zone *i.e.* $\{Inside \cup Neigh\}$, or outside the zone *i.e.* $\{Neigh \cup Far\}$. Because of the transition $\{Inside \cup Neigh\}$, Ω_{obs} is more detailed than Ω_{pre}. The set of focal elements for the observation is then

$$\xi_{\Omega_{obs}} = \{Inside, Inside \cup Neigh, Neigh \cup Far, \Omega_{obs}\}.$$

One can say that a single binary PIR output can discern only $Inside$ and $\overline{Inside}$. However, note that we rather deal with a sensor network, hence, several binary outputs can be received within a time window that may refer to either a zone and/or a transition between zones. In fact, since the prediction requires a motion model which is defined w.r.t a time window, the measurement data will be harvested within the same time window. This can easily lead to receiving several binary PIR outputs from different zones within the same time window. Note that taking $\Omega = \{Zone(1), ...Zone(n)\}$ as a common FoD is not consistent in our case since the prediction must be computed only for each zone separately, *i.e.* prediction cannot *directly* discern all zones. Moreover, the cardinal of such FoD increases with the number of zones and may lead to computational issues since the computational cost during the combinations depends on the cardinality of the FoD [18].

B. Mass functions construction

1) Prediction mass functions: The prediction step relies on the human motion model along with the past location probability results at $t-1$ to predict the probability of presence in each zone for the current time t. The set of focal elements of Ω_{pre} is $\xi_{\Omega_{pre}} = \{Inside, \overline{Inside}\}$. The mass function $m_{pre}^{\Omega_{pre}}$ of these focal elements, which is then a Bayesian mass function, is modeled for each $Zone(i)$ as follow:

$$m_{pre}^{\Omega_{pre}}(Inside, i) = (P_{i,t-1}) \cdot \gamma_{stay} + \sum_{j=1}^{N_j}(P_{j,t-1}) \cdot \gamma_{move} + \sum_{k=1}^{N_k}(P_{k,t-1}) \cdot \gamma_{jump} \quad (14)$$

$$m_{pre}^{\Omega_{pre}}(\overline{Inside}, i) = 1 - m_{pre}^{\Omega_{pre}}(Inside, i), \quad (15)$$

where N_j (*resp* N_k) is the number of Neighbor (*resp* Far) zones of $Zone(i)$. Besides, $(P_{i,t-1}), (P_{j,t-1})$ and $(P_{k,t-1})$ are respectively the past probability of presence in $Zone(i)$, in its neighbor zones $Zone(j)$ and in its further zones $Zone(k)$. $\gamma_{stay}, \gamma_{move}$ and γ_{jump} are the parameters of the motion model and represent respectively the probability of staying within the same zone, moving to a neighbor zone or jumping to a far zone. The probability γ_{move} should generally be smaller than γ_{stay} and the probability γ_{jump} should be far smaller but not null *i.e.* $\gamma_{stay} > \gamma_{move} >> \gamma_{jump}$. This rule is inspired from the following reasoning: Firstly, the chances that a person jumps to a far zone within one second time window are null, however, γ_{jump} should be very small but not zero to allow to recover from a failure at next time windows as shown in [6]. Secondly, γ_{move} and γ_{stay} should be equal in theory since if a person is inside a $Zone(i)$ at $t-1$, then, he/she could either stay in the same zone or move to a neighbor zone at the next time t. Nevertheless, even if the person decides to move into a neighbor zone, the person could be either *completely* inside the neighbor zone, or still transiting between the two zones due to the uncertainty on the FoV of the PIR sensors. Since a transition is regarded as being inside both zones, then, even if the person decides to move to a neighbor zone at next time, there is a chance that he/she will partially be inside the previous zone (*partially stay*). In other words, the possibility of transition is included in γ_{stay}. Consequently, the probability γ_{stay} should be higher than γ_{move} in practice.

Note that no automatic way exists to estimate these parameters, nevertheless, changing the values of these parameters does not greatly impact the localization results as long as the rule $\gamma_{stay} > \gamma_{move} >> \gamma_{jump}$ is satisfied as shown further in Sect. V-B. Besides, this model is also used in [6] and [14], therefore, it will be more consistent next to compare the results of the TBM localization algorithm w.r.t the ones of the previous algorithm [14].

2) Observation mass functions: For each $Zone(i)$, the masses $m_{obs}^{\Omega_{obs}}$ of the focal elements are modeled over Ω_{obs} as follow:

- $m_{obs}^{\Omega_{obs}}$ over $Inside$ and $Neigh \cup Far$:

$$m_{obs}^{\Omega_{obs}}(Inside, i) = \frac{N_{Act}(i) \cdot \mu(i)}{N_{Cov}(i) \cdot N_{Tot\_act}} \quad (16)$$

$$m_{obs}^{\Omega_{obs}}(Neigh \cup Far, i) = \frac{N_{Non\_act}(i) \cdot \mu(i)}{N_{Cov}(i) \cdot N_{Tot\_act}} \quad (17)$$

where $N_{Act}(i)$ (*resp* $N_{Non\_act}(i)$) represents the number of activated (*resp* non activated) sensor(s) in $Zone(i)$. N_{Tot_act} is the total number of activated sensors of the whole sensor network at time *t*. $N_{Cov}(i) = N_{Act}(i) + N_{Non\_act}(i)$ is the number of sensor(s) covering $Zone(i)$. In fact, the belief of being $Inside$ (*resp* $Neigh \cup Far = \overline{Inside}$) a $Zone(i)$ depends on the number of its activated $N_{Act}(i)$ (*resp* non activated $N_{Non\_act}(i)$) sensor(s) at time window *t*, against both the number of sensor(s) covering $Zone(i)$ *i.e.* $N_{Cov}(i)$ and the total activated sensors in the whole networks N_{Tot_act} at time window *t*. Nevertheless, to obtain appropriate mass functions, for

example, a unit mass $m_{obs}^{\Omega_{obs}}(Inside, i)$ in $Zone(i)$ when all its covering sensor(s) are activated and when their number is equal to the number of total activated sensor(s) (*i.e.* $m_{obs}^{\Omega_{obs}}(Inside, i) = 1$ when $N_{Act}(i) = N_{Tot\_act}$), we add the normalization parameter $\mu(i)$. The latter corresponds to $N_{Act}(i)$ since it will be simplified with N_{Tot_act} in such example, and omitting it may lead to inconsistent mass functions generation.
Indeed, mass normalization is sometime necessary, for example, in [19] authors added a normalization factor during mass functions generation to obtain appropriate mass functions. Note that if the number of activated sensors is null in a $Zone(i)$ and if the total number of activated sensors is not null, then the $m_{obs}^{\Omega_{obs}}(Neigh \cup Far, i)$ is set to one. Also, if there is no measurement at time *t*, we do not compute observation mass functions since we will keep the previous location results.

- $m_{obs}^{\Omega_{obs}}$ for $Inside \cup Neigh$ during a transition:
Transition between zones can be seen as being $Inside$ several zones. In fact, a transition between two zones $Inside(i) \cup Neigh(i)$ can be seen as $Inside(i) \cup Inside(j)$ with j related to $Zone(j)$ which is the neighbor zone of $Zone(i)$ involved in the transition. Therefore, constructing mass function for a transition $Inside \cup Neigh$ is similar to constructing a mass for $Inside$ for several zones. Consequently, the transition mass function depends on the number of activated sensor(s) in each involved zone, against both the number of sensor(s) covering each zone and the total activated number at the time window *t*. This leads to (18), which shares similar parameters with (16), as follows:

$$m_{obs}^{\Omega_{obs}}(Inside \cup Neigh = Transition, i) = \frac{(N_{Act}(i) + N_{Act}(j)) \cdot \mu_{transit}(i \cup j)}{(N_{Cov}(i) +_{Cov} (j)) \cdot N_{Tot\_act}} \quad (18)$$

where $\mu_{transit}(i \cup j)$ is the normalization parameter for transitions defined as:

$$\mu_{transit}(i \cup j) = (N_{Act}(i) + N_{Act}(j)) - N_{Common}$$

N_{Common} is the number of common activated sensors between zones involved in the transition and we subtract it to have $\mu_{transit}(i \cup j) \leqslant N_{Tot\_act}$ (accordingly, to have $m_{obs}^{\Omega_{obs}}(Inside \cup Neigh, i) \leqslant 1$). The mass in (18) corresponds to a transition mass function involving two zones, nevertheless, it can be extended if there are additional zones involved.
Note that for the zones involved in a transition, their corresponding $m_{obs}^{\Omega_{obs}}(Inside)$ and $m_{obs}^{\Omega_{obs}}(Neigh \cup Far)$ are set to zero, since during a transition we cannot discern between $Inside$ and $Neigh \cup Far$ for involved zones.

- $m_{obs}^{\Omega_{obs}}$ over Ω_{obs}:
In a non-transition case, we have $m_{obs}^{\Omega_{obs}}(Inside, i) + m_{obs}^{\Omega_{obs}}(Neigh \cup Far, i) \leqslant 1$. Also, during a transition case we have $m_{obs}^{\Omega_{obs}}(Inside \cup Neigh, i) \leqslant 1$. Therefore, to get $\sum_{H \in 2^{\Omega_{obs}}} m_{obs}^{\Omega_{obs}}(H) = 1$ in both cases we define:

$$m_{obs}^{\Omega_{obs}}(\Omega_{obs}, i) = 1 - \Big(m_{obs}^{\Omega_{obs}}(Inside \cup Neigh, i) + m_{obs}^{\Omega_{obs}}(Neigh \cup Far, i) + m_{obs}^{\Omega_{obs}}(Inside, i)\Big) \quad (19)$$

C. Appropriate discounting factor and mass weighting

When fusing data from different sources, it is judicious to weight the provided data w.r.t to the confidence of its corresponding source. In our case, the observation source is less reliable than the prediction source, therefore, the observation mass functions $m_{obs}^{\Omega_{obs}}$ are weighted using the discounting defined by *Shafer* [16] as shown in (20).

$$\begin{cases} {}^{\alpha_{obs}}m_{obs}^{\Omega_{obs}}(C) = (1 - \alpha_{obs}) \cdot m_{obs}^{\Omega_{obs}}(C), \forall C \subsetneq \Omega_{obs} \\ {}^{\alpha_{obs}}m_{obs}^{\Omega_{obs}}(\Omega_{obs}) = (1 - \alpha_{obs}) \cdot m_{obs}^{\Omega_{obs}}(\Omega_{obs}) + \alpha_{obs} \end{cases} \quad (20)$$

where ${}^{\alpha_{obs}}m_{obs}^{\Omega_{obs}}$ is the weighted mass. α_{obs} is the discounting factor and $(1 - \alpha_{obs})$ is the confidence in the observation.

Nevertheless, the choice of an appropriate value for the discounting factor is challenging. This value can be estimated *a priori* through a learning phase *e.g.* [20] or evaluated *a posteriori* after treating beliefs of the different sources based on distances [21] and conflict measure [22].

In our case, the observation source $m_{obs}^{\Omega_{obs}}$ is reliable but not at 100% (*e.g* due to delayed data within a time window, false positive/negative, ... etc.) let say $(1 - \alpha_{obs}) \in [0.7, 0.95]$ *i.e.* $\alpha_{obs} \in [0.05, 0.3]$. Unfortunately, choosing an inappropriate value of α_{obs} in this range can lead to counter-intuitive results during DS normalization over each zone, hence, leading to inconsistent location results as shown further in Example01 of *Appendix B*. Note that this counter-intuitive issue in our case is different from the famous *Zadeh's* counter-intuitive issue [23]. Indeed, *Zadeh's* issue can occur when a source has a so called *dictatorial power* as shown in [24], however, in our case the counter-intuitive issue may occur since the belief $m_{pre \cap obs}(Inside, Z_i)$ of some zone(s) may increase significantly compared to the other zones during DS normalization since each zone has its own corresponding mass of empty set. Consequently, relying on a priori learning phase [20] or on a posteriori evaluation as in [21] [22] may not necessarily lead to the appropriate discounting, since in our case, this appropriateness does, not only depend on the reliability of the source, but it also depends on the behavior of the DS normalization function as illustrated in *Appendix B*. Therefore, the discounting factor(s) of information source(s) should satisfy the constraint (21) bellow (See *Appendix B* for demonstration).

$$(1 - \alpha_1) \cdot .. \cdot (1 - \alpha_n) \leq max(m_\phi) \quad (21)$$

where: n is the number of sources to be discounted. $max(m_\phi)$ is the maximum value that mass of empty set of each zone should not exceed to avoid counter-intuitive results.

As a special case, if the *n* sources are considered *equally* reliable, this leads to $(1 - \alpha)^n \leq max(m_\phi)$ which means that they should be equally discounted with $\alpha \geq 1 - \sqrt[n]{max(m_\phi)}$ to ensure avoiding counter intuitive results. Finally, we show

in *Appendix B* that $max(m_\phi) \approx 0.75$, and since we discount only the observation source *i.e. n = 1*, hence, the appropriate α_{obs} for observation should satisfy the following:

$$1 - \alpha_{obs} \leqslant max(m_\phi) \approx 0.75 \Rightarrow \alpha_{obs} \geqslant 0.25 \quad (22)$$

We take $\alpha_{obs} = 0.25$ to maximize beliefs from observation.

D. Combination and state filtering

We should note that prediction and observation are independent sources of evidence since the construction of the prediction mass functions depends only on the human motion model and the past results at $t-1$ whatever the state of the sensors (*i.e.* of the observation mass functions) at the current time t.

To combine prediction with observation, the mass functions must be defined over the same FoD. The challenge here is on which FoD should we combine. At first time, we combine prediction and observation masses over Ω_{obs} since otherwise we will loose the transition information. Consequently, the prediction mass functions $m_{pre}^{\Omega_{pre}}$ must be redefined over Ω_{obs} using the *vacuous extension* defined in (4) as follows:

$$\begin{aligned} m_{pre}^{\Omega_{pre}\uparrow\Omega_{obs}}(Inside, i) &= m_{pre}^{\Omega_{pre}}(Inside, i), \\ m_{pre}^{\Omega_{pre}\uparrow\Omega_{obs}}(Neigh \cup Far, i) &= m_{pre}^{\Omega_{pre}}(\overline{Inside}, i). \end{aligned}$$

We use DS combination rule to combine the prediction with the observation. Nevertheless, during a transition the DS normalization may cause a problem since the zones involved in the transition will have the null mass of the empty set (hence no DS normalization) in contrary to the rest of the zones, and this can further impact the location results. To cope with this issue, we switch to the disjunctive rule, known as *the prudent* rule, during a transition since the disjunctive rule does not induce the mass of the empty set during the combination. Therefore, all zones will be treated judiciously during a transition whether it is involved in the transition or not. The *a posteriori* combined mass is:

$$m_{1,2}^{\Omega_{obs}} = m_{pre}^{\Omega_{pre}\uparrow\Omega_{obs}} \odot {}^{\alpha}m_{obs}^{\Omega_{obs}} \quad (23)$$

where dot in $\odot$ is replaced by $+$ when using DS rule, and by $\cup$ when using the disjunctive rule during a transition.

Indeed, DS rule may lead to counter intuitive results in several cases. The famous case is *Zadeh's* [23] example which shows counter intuitive results when the mass of the empty set is too high. However, in [24] it is shown that counter-intuitive results can occur at any level of conflict in case where a source has a so-called *dictatorial power*. Fortunately, such dictatorial power is not present in our case since $Pl_{pred}^{\Omega_{obs}}(C) \neq 0$ and $Pl_{obs}^{\Omega_{obs}}(C) \neq 0 \; \forall C \in \xi_{\Omega_{obs}}$. In fact, since $m_{pre}^{\Omega_{pre}\uparrow\Omega_{obs}}(Inside)$ is never null neither equal to 1, hence, $m_{pre}^{\Omega_{pre}\uparrow\Omega_{obs}}(Neigh \cup Far)$ is also never null and $Pl_{pred}^{\Omega_{obs}}(C) \neq 0 \; \forall C \in \xi_{\Omega_{obs}}$. Also, since the observation mass functions are discounted, we will always have ${}^{\alpha}m_{obs}^{\Omega_{obs}}(\Omega_{obs}) \neq 0$, hence, $Pl_{obs}^{\Omega_{obs}}(C) \neq 0 \; \forall C \in \xi_{\Omega_{obs}}$. Consequently, the dictatorial power issue is not present in both sources and there is no reason to use another combination rule (*e.g.* $PCR5$) as an alternative to DS rule during a non-transition.

Nevertheless, the only issue that occurs during transitions is that the *a posteriori* $m_{1,2}^{\Omega_{obs}}(Inside, i)$ will increase for the non-involved zones during DS normalization (since their $m_{1\cap2}^{\Omega_{obs}}(Inside, i)$ will be multiplied by the DS normalization factor to remove the induced mass of the empty set) which is not the case for the involved zones. Indeed, *a posteriori* will never increase for the involved zones since their mass of empty set is null by default (because $m_{obs}^{\Omega_{obs}}(Inside, i) = 0 = m_{obs}^{\Omega_{obs}}(Neigh \cup Far, i)$ as evoked in IV-B) and this is not fair since it may lead to inappropriate results when normalizing (*i.e.* increasing) the $m_{1\cap2}^{\Omega_{obs}}(Inside, j)$ of the non-involved zones as shown in *Appendix A*. One can say that we should use the conjunctive rule during transition, unfortunately, this is not possible since we consider that the FoD is exhaustive (*i.e.* a closed world).

Consequently, the appropriate combination rule for the transition case is the disjunctive rule despite of being less informative than DS rule.

E. Location probability distribution

To have a consistent comparison with our previous work, we need to transform the *a posteriori* mass function results to a location probability distribution P (with $P(\overline{Inside}) = 1 - P(Inside)$). This requires two operations. The first one is the projection of the *a posteriori* combined mass obtained in (23) over Ω_{pre} as follows:

$$m_{1,2}^{\Omega_{pre}} = m_{1,2}^{\Omega_{obs}\downarrow\Omega_{pre}} \quad (24)$$

Projection in (24) is obtained using the inner reduction. In fact, during a transition, the *a posteriori* mass obtained using the disjunctive rule $m_{1\cup2}^{\Omega_{obs}}(Inside \cup Neigh)$ can be allocated either to $m_{1\cup2}^{\Omega_{pre}}(Inside)$ if using the inner reduction, or to $m_{1\cup2}^{\Omega_{pre}}(\overline{Inside})$ if using the outer reduction. However, we have noticed previously in IV-B that a transition $Inside \cup Neigh$ corresponds rather to $Inside$ in several zones, hence, for each zone it is rather judicious to allocate $m_{1\cup2}^{\Omega_{obs}}(Inside \cup Neigh)$ to $m_{1\cup2}^{\Omega_{pre}}(Inside)$ and not to $m_{1\cup2}^{\Omega_{pre}}(\overline{Inside})$. Also, when there is no transition, inner reduction leads to the same mass as the outer reduction since only $m_{1\oplus2}^{\Omega_{obs}}(Neigh)$ can make a difference (it can be either allocated to $m_{1\cup2}^{\Omega_{pre}}(\overline{Inside})$ if outer reduction, or to the empty set if inner reduction). Nevertheless, $m_{1\oplus2}^{\Omega_{obs}}(Neigh)$ is null when there is no transition because it is obtained by $m_{1\oplus2}^{\Omega_{pre}}(Neigh \cup Far) \cdot m_{1\oplus2}^{\Omega_{obs}}(Inside \cup Neigh)$ and $m_{1\oplus2}^{\Omega_{obs}}(Inside \cup Neigh)$ is null in non-transition case.

The second operation transforms the projected mass functions into probabilities using the pignistic transform $BetP_i^{\Omega_{pre}}(Inside)$ over each $Zone(i)$ as follows:

$$P(Inside, i) = BetP^{\Omega_{pre}}(Inside, i) = \frac{1}{1 - m_{\oplus}^{\Omega_{pre}}(\phi)} \cdot \left(m_{1,2}^{\Omega_{pre}}(Inside, i) + \frac{m_{1,2}^{\Omega_{pre}}(\Omega_{pre}, i)}{2} \right) \quad (25)$$

where $m_{1,2}^{\Omega_{pre}}$ is the combined mass and $m_{\oplus}^{\Omega_{pre}}(\phi)$ is the mass of the empty set after combination and projection.

Algorithm 1 Get the location probability distribution

Require: $\Omega_{pre} = \{Inside, \overline{Inside}\}$
$\Omega_{obs} = \{Inside, Neigh, Far\}$
$\xi_{\Omega_{pre}} = \{Inside, \overline{Inside}\}$
$\xi_{\Omega_{obs}} = \{Inside, \underbrace{Inside \cup Neigh}_{Transition}, \underbrace{Neigh \cup Far}_{\overline{Inside}}, \Omega_{obs}\}$
for each time step t **do**
for each $Zone(i)$ **do**
1) Compute mass functions:
get $m_{pre}^{\Omega_{pre}}(H,i) \quad \forall H \in \xi_{\Omega_{pre}}$ using (13) (14).
get $m_{obs}^{\Omega_{obs}}(C,i) \quad \forall C \in \xi_{\Omega_{obs}}$ using (15)-(18).
2) Weight observation mass functions $m_{obs}^{\Omega_{obs}}$:
get ${}^{\alpha}m_{obs}^{\Omega_{obs}}(C,i) \quad \forall C \in \xi_{\Omega_{obs}}$ using (19).
3) State filtering:
3.a) Redefine $m_{pre}^{\Omega_{pre}}$ over Ω_{obs} using *vacuous* extension:
$m_{pre}^{\Omega_{pre}\uparrow\Omega_{obs}}(C,i) = \begin{cases} m_{pre}^{\Omega_{pre}}(H,i) \text{ if } C = \rho(H) \\ 0 \quad \text{else} \end{cases}$
$\forall C \in \xi_{\Omega_{obs}}, \forall H \in \xi_{\Omega_{pre}}$
3.b) Combine $m_{pre}^{\Omega_{obs}}$ with $m_{obs}^{\Omega_{obs}}$ using (20):
if Transition measurement case **then**
$m_{1,2}^{\Omega_{obs}}(C,i) = m_{pre}^{\Omega_{pre}\uparrow\Omega_{obs}}(C,i) \cup {}^{\alpha}m_{obs}^{\Omega_{obs}}(C,i)$
else
$m_{1,2}^{\Omega_{obs}}(C,i) = m_{pre}^{\Omega_{pre}\uparrow\Omega_{obs}}(C,i) \oplus {}^{\alpha}m_{obs}^{\Omega_{obs}}(C,i)$
end if
$\forall C \in \xi_{\Omega_{obs}}$
4) Location probability distribution:
4.a) Redefine $m_{1,2}^{\Omega_{obs}}$ over Ω_{pre} using (22):
$m_{1,2}^{\Omega_{obs}\downarrow\Omega_{pre}}(H,i) = \sum_{C \in \xi_{\Omega_{obs}}, \rho(H) \subseteq C} m_{1,2}^{\Omega_{obs}}(C,i)$
4.b) Presence probability for each $Zone(i)$ using (24):
$P(Inside,i) = BetP^{\Omega_{pre}}(Inside,i)$
4.c) Normalize the probability distribution using (25):
$P_{Norm}(Inside,i) = \frac{P(Inside,i)}{\sum_{k=1}^{N_z} P(Inside,k)}$
end for
end for

Note that when using DS combination, the mass of the empty set is set to zero after DS normalization in the credal level. Also, when using the disjunctive combination, this mass is also null since it cannot be obtained. Hence, at pignistic level, $m_{\oplus}^{\Omega_{obs}}(\phi) = 0$. Finally, $m_{\oplus}^{\Omega_{pre}}(\phi) = m_{\oplus}^{\Omega_{obs}}(\phi)$ during the projection, therefore, $m_{\oplus}^{\Omega_{pre}}(\phi) = 0$ at pignistic level.

Location probability for each zone $P(Inside,i)$ becomes :

$$P(Inside,i) = BetP^{\Omega_{pre}}(Inside,i) = \left(m_{1,2}^{\Omega_{pre}}(Inside,i) + \frac{m_{1,2}^{\Omega_{pre}}(\Omega_{pre},i)}{2} \right) \quad (26)$$

To compare the TBM based results with our previous work [14], we need a *normalized* location probability distribution which is obtained as follows for all zones (i)

$$P_{Norm}(Inside,i) = \frac{P(Inside,i)}{\sum_{k=1}^{N_z} P(Inside,k)} \quad (27)$$

where N_z is the total number of zones.

Finally, the different steps of the localization algorithm are summarized in the **Algorithm 1**.

V. Experiment Results and Discussion

First of all, to show the interest of the transition handling, we have performed a simple scenario $Scenario01$ shown in Fig.4.a) with $deployementA$. The results of this scenario, which are detailed in V-A, highlights the caution of the TBM method during transitions and shows its interest for subsequent decision-making study. Secondly, we have tested both localization methods for two scenarios with different deployments and configurations as shown in V-B.

The measurements are collected based on a one second time window so that the fusion of the observation with the prediction would be consistent, since if the time window is very large *e.g.* ten seconds, the person can move to any far zone in the next time window and the prediction defined in (14) will not be reasonable. Also, to have a fair comparison, the same initialization was taken as equi-probable for both methods. An example of a placed PIR sensor along with its multiplex mask is shown in Fig.3, and it corresponds to the *Red* sensor in Fig.1.b) and in Fig.1.c).

The proposed experiment scenarios are shown in Fig.4. In $Scenario01$, the person has left the bed to reach the table (*e.g.* to take a glass of water from the table) then went on his/her way to sit down on the chair in the bed room (*e.g.* to watch TV). To further test our novel method, we have added the $Scenario02$ which is more complete and solicits almost all the zones of interest.

A. Results highlighting the interest of transition handling

From Fig.5.a) we can see that the initialization is the same for both algorithms (each zone has a probability of $0.076 = 1/13$). The person started moving at $t = 6s$ and reached $zone3.b$ at $t = 10s$ which corresponds to Fig.5.b). During the next time window $t = 11s$, the person was transiting between $zone3.b$ and $zone6$ and we can see from Fig.5.c) that our novel TBM algorithm results are more consistent compared to our previous algorithm results. In fact, the received measurement at $t = 11s$ is $Yellow, Orange$ and $Green$ sensors are activated and such measurement can correspond either to a transition ($zone3.b \cup zone6$) or to a transition ($zone3.b \cup zone3.a = zone4$ with $Green$ is in false positive). Hence, it is clear that there is some uncertainties over these

(a) Left side view (b) Right side view

Fig. 3: A placed PIR sensor with our multiplex mask

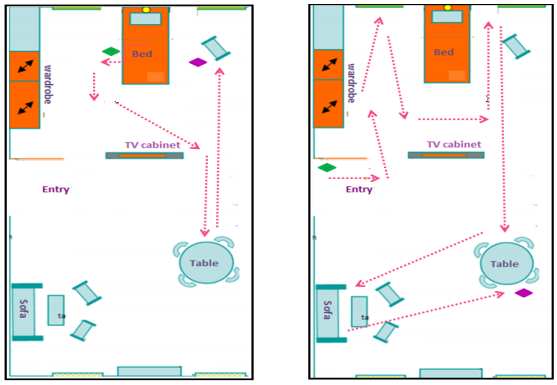

(a) Scenario 01 (b) Scenario 02

Fig. 4: Experiment scenarios. Green lozenge is the starting position and purple lozenge is the ending one.

zones and in this situation the TBM based algorithm is prudent since it did not really prefer a zone over the involved zones due to the disjunctive rule which is less informative. Nevertheless, the involved zones have higher probabilities than the non-involved zones and the maximum probability corresponds to $zone3.b$ which is consistent w.r.t the ground truth. On the other hand, our previous Bayesian based algorithm did not handle the uncertainty induced during the transition since it has preferred $zone4$ (high difference of probability between $zone4$ and $zone6$) which is not consistent w.r.t the ground truth since the person was rather transiting between $zone3.b$ and $zone6$ and he was not inside $zone4$.

Our previous algorithm may recover from such transition errors depending on the next situations, for example, at $t = 22s$ we can see from Fig.5.d) that the previous algorithm has recovered from the transition error caused at $t = 11s$. Unfortunately, such recovering requires time and depends on the next motions and this might not be always good for subsequent decision making study. Indeed, after $t = 22s$ the person left $zone9$ to go to $zone2$ and at $t = 27s$ the person was transiting between $zone3.a \cup zone2$ to reach the chair. At this $t = 27s$ time window, we can see from Fig.5.e) that TBM results are consistent since $zone3.a$ and $zone2$ have the highest probabilities in contrary to the previous algorithm results where the highest probabilities are in $zone3.a$ and $zone4$. This error in our previous algorithm at $t = 27s$ has induced other errors at the next time window $t = 28s$ where the person has reached the chair in $zone2$. We can see from 5.f) that at $t = 28s$ the TBM algorithm results are consistent, however, the previous algorithm results are not consistent since probability in $zone2$ is not the highest yet. This is due to the erroneous results caused by the successive transitions from $t = 22s$ to $t = 27s$.

From $t = 28s$ to $t = 34s$ no sensor was activated since no sufficient motion has been performed, therefore, the same location results are kept without updating the location results *i.e.* the probabilities. At $t = 35s$ the person performed a sufficiently large motion in the chair and the $Black$ sensor was activated, at this moment, the previous algorithm started recovering and we can see from 5.g) that $zone2$ has the highest probability in both algorithms. Nevertheless, the probability of $zone2$ for the previous algorithm is not significant yet w.r.t $zone3.a$ (small difference of probability between $zone2$ and $zone3.a$) and the previous algorithm has to wait for another motion to get more significant probabilities. Hence, for the time interval $t = 27s$ to $t = 35s$ we can say that the person was in $zone2$ relying on TBM algorithm results, however, we cannot conclude yet if we rely on the previous algorithm results. Consequently, if a decision has to be made within this time interval $[27-35]$, it can be easily made using TBM results since the person was in the same zone during this interval, however, the location results was not stable and inconsistent when using our previous algorithm for this same time interval. Note that for both algorithms, some location errors may occur (*e.g.* due to successive false positives, missing data during time window sampling, ...etc.), however, both can recover from such errors once the measurements at next time window(s) are correct.

B. Impact of durable sensors faults, deployment, and setting

To evaluate both methods over different setups and scenarios, we compute the localization error rate as follows:

$$Error\,rate = \frac{N_{False}}{N_{all}} \cdot 100 \tag{28}$$

where N_{False} is the number of measurement time windows when the relatively highest probability is assigned to a wrong zone. N_{all} is the total number of time windows.

1) Impact of durable sensors faults: False positive and false negative are well known faults for PIR sensors. In our case, an additional aspect of these faults is pointed out which depends on the duration of the fault within the sensor network. This aspect concerns *fleeting* fault(s) and *durable* fault(s). A *fleeting* fault is a false positive/negative which lasts for one time window/ Such kind of faults could be overcome through filtering.

A *durable* fault is a false positive/negative which lasts for several successive time windows. For example, when a person enters $Zone09$ she will be localized properly as it was the case in Fig.5.d). However, if the person performs successive small motions that activate only $Purple$ sensor, a *durable* fault will be induced and the probability will gradually decrease in $Zone09$ and increase in $Zone05$. Nevertheless, when the person performs a large motion, she will be localized again in $Zone09$.

We can see from Table I and II that the error rate of the TBM method is always smaller than the error rate of our previous method. Also, when omitting the errors caused by the *durable* faults, the error rate of the TBM method becomes much smaller (around 5% or less for almost all cases). This is not the case for the previous method since the error rate is still high because of the additional errors caused during transitions. Finally, the error rates of the TBM method are smaller than the sensors network fault rate[4] .

[4]Total sensor network faults rate is obtained by checking the consistency of the received measurements of each time window of the data set w.r.t ground truth.

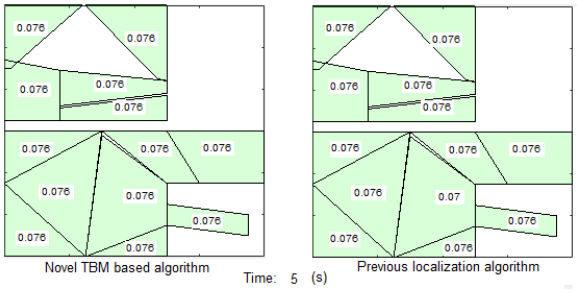

(a) At t = 5(s) initialization (no motion yet)

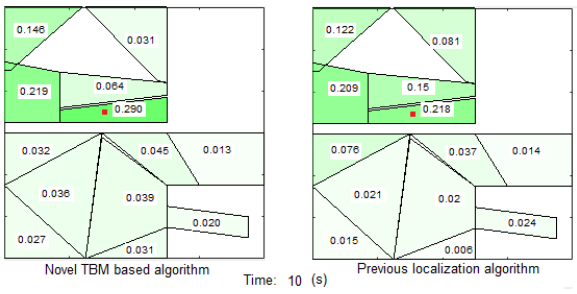

(b) At t = 10(s) person is in Zone3.b

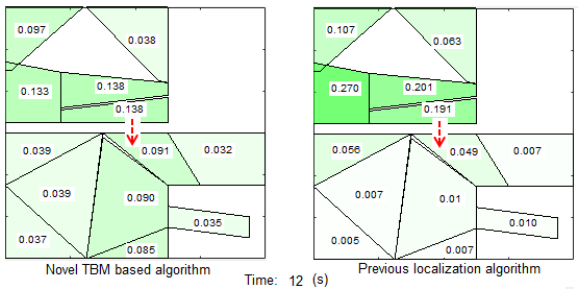

(c) At t = 12(s) the person is transiting between zone3.b to zone6

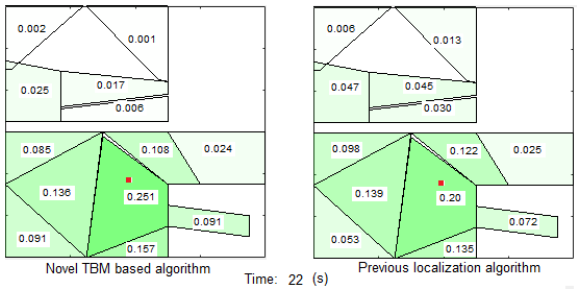

(d) At t = 22(s) the person is about to quit zone

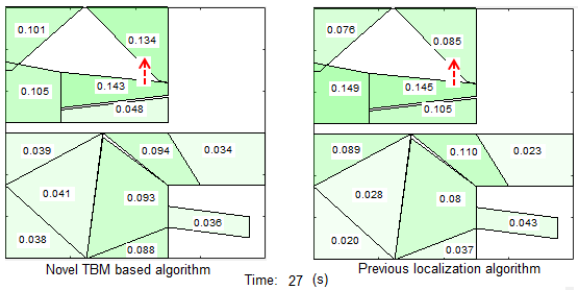

(e) At t = 27(s) the person is transiting between zone3.a and zone2

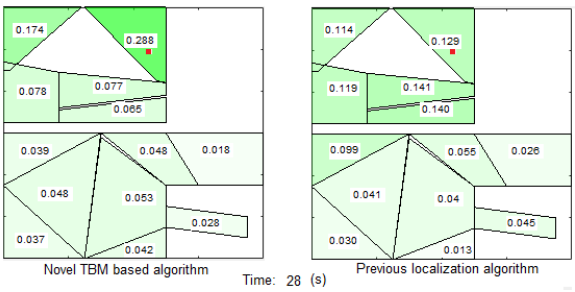

(f) At t = 28(s) the person entered zone2

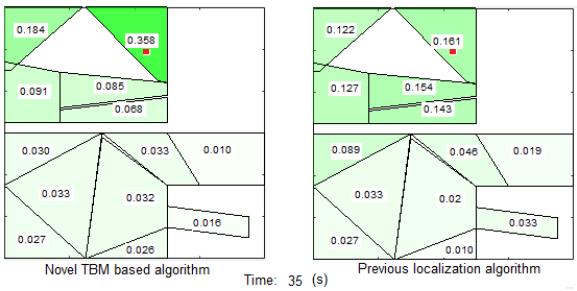

(g) At t = 35(s) the person sits on the chair in zone2

Fig. 5: Comparison of the novel TBM algorithm results with the results of our previous algorithm [14]. Red square corresponds to the person's position inside a zone while the red arrow corresponds to the transition.

2) Impact of sensors deployment: Depending on the case of study, PIR sensors deployment may reduce the sensors fault rate. For example, in [12] authors showed that an adequate sensors deployment can improve the tracking performance. In [25], authors showed that different sensor nodes orientations can lead to different tracking accuracy. Nevertheless, in both studies, the location accuracy concerned the error in position coordinates and not the probability of presence in some defined zones of interests. Also, their experiments did not have severe constraints on sensors placement (square areas are considered and no zone of interest constraints).

In our case of study, the sensors can be placed only in some specific places within the smart-home due to architectural constraints (windows, furniture, .. etc.) in one hand, and due to the zones of interest covering in the other hand. Therefore, an optimal sensors deployment is not always easy to implement. Moreover, location errors for a specific sensors deployment may increase or decrease depending on the considered scenario along with the *durable* sensors faults caused by the nature of human motion during the scenario. In fact, $deploymentA$ shows less location errors compared to $deploymentB$ in the case of $scenario01$ which is the opposite in the case of

$scenario02$. Consequently, the location errors rate related to a sensors deployment depends also on the scenario and on the nature of the human motions, and these last should be considered when looking for optimal deployment.

3) Impact of parameters setting: In a first a part, we will analyze the impact of the parameters setting within a same scenario to check the consistency of the rule $\gamma_{stay} > \gamma_{move} >> \gamma_{jump}$. In the second part, we will analyze the impact of the parameters setting for different scenarios.

For the first part, we consider the results of the $scenario01$ shown in Table.I. We can see from this table that location the error rates increased relatively when $\gamma_{stay} = \gamma_{move}$ and that they are still high even when omitting errors caused by durable faults. This is because when $\gamma_{stay} = \gamma_{move}$, the TBM method (and also our previous method) becomes less robust against fleeting faults. For this reason, and as explained in IV-B1, we take the rule $\gamma_{stay} > \gamma_{move} >> \gamma_{jump}$ in practice.

Now, let us consider that this rule is satisfied (*i.e.* by considering only the two settings $\gamma_{stay} = 0.65$ and $\gamma_{stay} = 0.85$). We can see from Table.I that the best location error rate is obtained with the setting $\gamma_{stay} = 0.85$ in the case of $scenario01$, however, the best error rate is rather obtained with $\gamma_{stay} = 0.65$ in the case of $scenario02$. From this analysis, one can say that the choice of the parameters values depends on the scenario, however, even for a same data set, the parameters setting may increase/decrease the location error rate caused by durable faults. For example, for the $scenario02$ with deployment B, the location errors caused by the durable faults was 10.5% for $\gamma_{stay} = 0.65$ and 9.2% for $\gamma_{stay} = 0.85$. In fact, we believe that the parameters values should change w.r.t to the nature of the human motion during a scenario, for example, we should increase γ_{stay} when a small motion is detected, and decrease it when a large motion is detected. We believe that such switching may reduce location errors caused by durable sensor faults, if these faults are detected, which constitutes a track for our next research.

Parameters values for $Scenario01$	Setup	**TBM Meth** Error rate %	**Previous Meth [14]** Error rate %
$\gamma_{stay} = 0.85$ $\gamma_{move} = 0.14$ $\gamma_{jump} = 0.01$	A	$6,6$	36
		3,3	**26**
	B	$13,1$	26
		5,2	**13**
$\gamma_{stay} = 0.65$ $\gamma_{move} = 0.34$ $\gamma_{jump} = 0.01$	A	10	33
		3,3	**23**
	B	$13,1$	26
		5,2	**13**
$\gamma_{stay} = 0.49$ $\gamma_{move} = 0.49$ $\gamma_{jump} = 0.02$	A	$13,3$	43
		6,6	**26**
	B	$21,1$	29
		13,2	**15**

TABLE I: Location-tracking error rates for $scenario01$. Numbers in bold represent the location-tracking error rate when omitting errors caused by durable faults.

Parameters values for $Scenario02$	Setup	**TBM Meth** Error rate %	**Previous Meth [14]** Error rate %
$\gamma_{stay} = 0.85$ $\gamma_{move} = 0.14$ $\gamma_{jump} = 0.01$	A	$18,4$	32
		5,2	**13,1**
	B	$14,4$	27
		5,2	**15,7**
$\gamma_{stay} = 0.65$ $\gamma_{move} = 0.34$ $\gamma_{jump} = 0.01$	A	$17,1$	28
		3,9	**14,4**
	B	$13,1$	21
		2,6	**10,5**
Sensors network faults rate	A	26.7 %	
	B	$22,3$ %	

TABLE II: Location-tracking error rates for $scenario02$. Numbers in bold represent the location-tracking error rate when omitting errors caused by durable faults.

C. Discussion

In V-A, we have shown how the TBM method is prudent during transitions and how its location results could be more significant for subsequent decision-making studies compared to our previous localization algorithm [14]. Also, we have shown, with different scenarios and setups in V-B, that the error rates of our previous method are always higher than the error rates of the TBM method. This is caused by the additional errors induced during the transitions between zones that our previous algorithm cannot handle.

We have seen that the TBM algorithm can deal with *fleeting* sensors network faults, however, it is sensitive to *durable* sensors faults. Also, we have shown that the localization performance does not only depend on the sensors deployment, but also on the scenario and nature of the human motions during the scenario. Since appropriate sensors deployment cannot always be achieved in practice, one should rather detect and deal with *durable* faults to increase the location-tracking performances which is the aim of our future work. Finally, the impact of the motion model parameters setting also depends on the scenario along with the nature of the human motions, and we believe that changing the values of the parameters setting depending on the nature of the human motions constitutes the track to deal with durable faults in our future work.

In our long-term project, other sensing modalities will be added and a decision making study will use our data fusion results. Consequently, our long-term studies concerns a state filtering by combining uncertain data from different modalities for a subsequent decision-making study. The TBM seems to be the coherent theoretical framework for our case since it has already shown its advantages in combining uncertain data for both decision making applications such as medical diagnosis [26] or target identification [27], and also in state filtering [28].

Finally, note that for multiple persons localization, it is more challenging when using overlapping binary PIR structure since received measurements obtained when multiple persons are moving may easily increase location errors. Indeed, *Bo Yang et al* pointed out this issue in [25] and solved it using classifiers with a learning phase [8] or relying on clustering [9]. Since other sensing modalities will be further used in our long-term project, hence, we will exploit multi-modal data fusion approach to deal with the multiple person issue without learning phases or clustering requirement.

VI. Conclusion

In this paper, we have firstly enhanced our previous multiplex binary localization approach to overcome the ambiguity in the detection of transitions between zones, by using a filtering technique based on the transferable belief model (TBM) instead of the Bayesian framework. Secondly, we have presented a new way for choosing an appropriate discounting factor to weight an information source w.r.t the other source(s), relying on the analysis of the Dempster-Shafer normalization function. The desired zones of interest are covered with a reduced number of sensors thanks to the overlapping multiplex structure. Our novel method is robust against fleeting sensor faults thanks to filtering, and against reasonable uncertainty on sensor's field of view (which is related to transition) thanks to the uncertainty handling using the TBM framework. Finally, experiments using commercialized single PIR sensors, with modified field of view, showed the advantages of the TBM method w.r.t our previous Bayesian method.

Our next work will consist in enhancing the location-tracking results by dealing with durable sensors faults, and addressing the location-tracking of multiple humans.

Appendix A
Illustrative Example with *Deployment A*

This example shows the inappropriate location results induced if we use the DS rule during a transition. Let's consider the transition $Z3.a \cup Z3.b$ where the person left $Z6$ to go to $Z2$. In this case, we will logically have: $m_{pre}^{\Omega_{pre}\uparrow\Omega_{obs}}(Inside, Z3.b) > m_{pre}^{\Omega_{pre}\uparrow\Omega_{obs}}(Inside, Z3.a) > m_{pre}^{\Omega_{pre}\uparrow\Omega_{obs}}(Inside, Z4)$. Let's say their values are: $m_{pre}^{\Omega_{pre}\uparrow\Omega_{obs}}(Inside, Z3.b) = 0.75$, $m_{pre}^{\Omega_{pre}\uparrow\Omega_{obs}}(Inside, Z3.a) = 0.6$, $m_{pre}^{\Omega_{pre}\uparrow\Omega_{obs}}(Inside, Z4) = 0.3$. Also, for the observation we assume that $Orange$ and $Yellow$ sensors are activated due to this transition, hence:

$$m_{obs}^{\Omega_{obs}}(Inside, Z4) = m_{obs}^{\Omega_{obs}}(Inside \cup Neigh, Z3.a) = m_{obs}^{\Omega_{obs}}(Inside \cup Neigh, Z3.b) = 1.$$

After observation and mass discounting, we obtain:

$$^{\alpha}m_{obs}^{\Omega_{obs}}(Inside, Z4) = {}^{\alpha}m_{obs}^{\Omega_{obs}}(Inside \cup NeighZ3.a) = {}^{\alpha}m_{obs}^{\Omega_{obs}}(Inside \cup NeighZ3.b) = 0.75$$
$$^{\alpha}m_{obs}^{\Omega_{obs}}(\Omega_{obs}, Z4) = {}^{\alpha}m_{obs}^{\Omega_{obs}}(\Omega_{obs}, Z3.a) = {}^{\alpha}m_{obs}^{\Omega_{obs}}(\Omega_{obs}, Z3.b) = 0.25$$

Conjunctive combination results are then:

$$m_{1\cap2}^{\Omega_{obs}}(Inside, Z3.b) = 0.75 > m_{1\cap2}^{\Omega_{obs}}(Inside, Z3.a) = 0.6 > m_{1\cap2}^{\Omega_{obs}}(Inside, Z4) = 0.3$$

With: $m_{1\cap2}^{\Omega_{obs}}(\phi, Z3.b) = 0 = m_{1\cap2}^{\Omega_{obs}}(\phi, Z3.a)$. However, $m_{1\cap2}^{\Omega_{obs}}(\phi, Z4) \neq 0 = 0.525$.

The conjunctive combination results are consistent with the proposed scenario. However, the DS normalization leads to:

$$m_{1\oplus2}^{\Omega_{obs}}(Inside, Z3.b) = 0.75. \text{ But: } m_{1\oplus2}^{\Omega_{obs}}(Inside, Z3.a) = 0.6 < m_{1\oplus2}^{\Omega_{obs}}(Inside, Z4) = 0.63$$

which is not consistent w.r.t the scenario.

Now, if we use the disjunctive combination we obtain:

$$m_{1\cup2}^{\Omega_{obs}}(Inside \cup Neigh, Z4) = 0.3$$
$$m_{1\cup2}^{\Omega_{obs}}(Inside \cup Neigh, Z3.a) = 0.42$$
$$m_{1\cup2}^{\Omega_{obs}}(Inside \cup Neigh, Z3.b) = 0.6$$

After inner reduction (24) we will get:

$$m_{1\cup2}^{\Omega_{pre}}(Inside, Z3.b) = 0.6 > m_{1\cup2}^{\Omega_{pre}}(Inside, Z3.a) = 0.42 > m_{1\cup2}^{\Omega_{pre}}(Inside, Z4) = 0.3$$

We can see that the disjunctive combination results are consistent w.r.t the scenario while considering the closed world property. For such a reason, we use the disjunctive combination instead of the DS combination during transitions.

Appendix B
Appropriate Discounting Factor

As evoked in IV-C, the appropriate value of α_{obs} is chosen by analyzing the behavior of the DS normalization function. In fact, if we analyze this function ($DS_{norm}(m_\phi) = \frac{1}{1-m_\phi}$) w.r.t the mass of the empty set m_ϕ as shown in Fig.6, we can see that $DS_{norm}(m_\phi)$ can be divided into three lines with different slopes which intersect around 0.75 for line A and line B, and around 0.9 for line B and line C. Since each zone will have its own mass of empty set $m_{pre\cap obs}(\phi, Z_i)$ during the non-transition cases (in transition cases there is no $m_{pre\cap obs}(\phi, Z_i)$ because the disjunctive rule is used), hence, the combined mass $m_{pre\cap obs}(Inside, Z_i)$ of each zone obtained by the conjunctive rule will increase during the DS normalization. Unfortunately, the masses $m_{pre\cap obs}(Inside, Z_i)$ will increase differently depending on the $m_{pre\cap obs}(\phi, Z_i)$ obtained for each zone, especially, this difference becomes more important and problematic when the different $m_{pre\cap obs}(\phi, Z_i)$ do not belong to the same line A as shown further in the Example01.

To minimize this difference during DS normalization accordingly to increase the consistency of localization results, it is necessary to ensure that the mass of the empty set of all zones will belong to the same line A. The limit of this line with line B corresponds to $m_\phi \simeq 0.75$, hence, if we choose $1 - \alpha_{obs} \leqslant 0.75$ (*i.e.* $\alpha_{obs} \geqslant 0.25$) we will be sure that m_ϕ of all zones will belong to the same line A. We choose only line A since its slope is very small, hence, the mass increasing during the DS normalization will not highly differ from a zone to another. Consequently, it will be unlikely then to obtain counter-intuitive results w.r.t the conjunctive combined masses after DS normalization.

Example01: This example shows the importance of having $m_{1\cap2}(\phi)$ of all zones belonging to the same line A. Let us consider the following scenario (with sensors $Deployment\ A$):

At time window $t-1$, the person is inside $zone05$. Accordingly, $m_{pre}(Inside, Z_8)$ at t is higher than $m_{pre}(Inside, Z_7)$ let's say:

$m_{pre}(Inside, Z_8) = 0.3 > m_{pre}(Inside, Z_7) = 0.05$.

At time window t the person enters $zone08$ but only $Green$ and Red sensors are activated ($Purple$ sensor is in false negative). With such measurement we obtain:

$$m_{obs}(Inside, Z_7) = 1,$$
$$m_{obs}(Neigh \cup Far, Z_7) = 0 = m_{obs}(\Omega, Z_7)$$
$$m_{obs}(Inside, Z_8) = 0.66,$$
$$m_{obs}(Neigh \cup Far, Z_8) = 0.33.\ m_{obs}(\Omega, Z_8) = 0$$

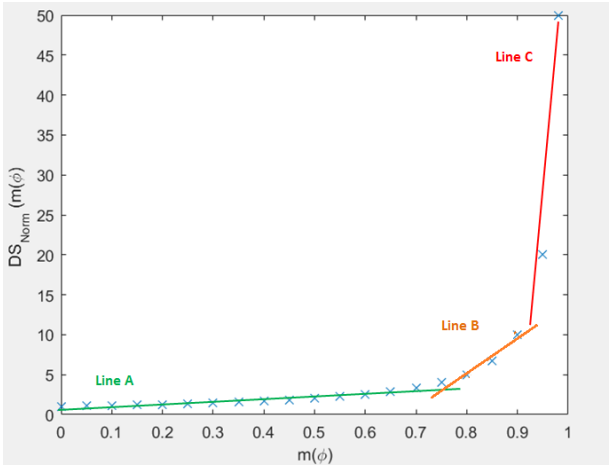

Fig. 6: DS_{Norm} factor evolution w.r.t $m(\phi)$

Now, let us analyze DS combination results for two cases, when $m_{pre\cap obs}(\phi, Z_7)$ and $m_{pre\cap obs}(\phi, Z_8)$ belong to different lines (case with $1-\alpha_{obs}=0.95$), and when they both belong to the same line A (case with $1-\alpha_{obs}=0.75$).

- If $\alpha_{obs}=0.05$ (*i.e.* $1-\alpha_{obs}=0.95$) :

$$^{\alpha_{obs}}m_{obs}(Inside, Z_7)=0.95.$$
$$^{\alpha_{obs}}m_{obs}(Neigh\cup Far, Z_7)=0.^{\alpha_{obs}}m_{obs}(\Omega, Z_7)=0.05.$$
$$^{\alpha_{obs}}m_{obs}(Inside, Z_8)=0.633.$$
$$^{\alpha_{obs}}m_{obs}(Neigh\cup Far, Z_8)=0.316.^{\alpha_{obs}}m_{obs}(\Omega, Z_8)=0.05.$$

Hence, conjunctive results are:

$$m_{pre\cap obs}(Inside, Z_7)=0.05$$
$$m_{pre\cap obs}(Inside, Z_8)=0.20$$

$$m_{pre\cap obs}(Inside, Z_7) < m_{pre\cap obs}(Inside, Z_8) \quad (29)$$

$$m_{pre\cap obs}(\phi, Z_7)\simeq 0.90\in Line\,C$$
$$m_{pre\cap obs}(\phi, Z_8)\simeq 0.53\in Line\,A$$

Conjunctive results in (29) are consistent w.r.t the scenario, however, DS normalization leads to (30):

$$m_{pre\oplus obs}(Inside, Z_7)=0.5$$
$$m_{pre\oplus obs}(Inside, Z_8)=0.42$$
$$m_{pre\oplus obs}(Inside, Z_7) > m_{pre\oplus obs}(Inside, Z_8) \quad (30)$$

This result in (30) is counter intuitive w.r.t (29) and to the scenario since at time t the person is inside $zone08$ and not inside $zone07$.

Now, let's see what happens when $m_{pre\cap obs}(\phi, Z_7)$ and $m_{pre\cap obs}(\phi, Z_8)$ belong to the same line A (*i.e.* when taking $1-\alpha_{obs}\leqslant 0.755$).

- If $\alpha_{obs}=0.25$ (*i.e.* $1-\alpha_{obs}=0.75$) :

$$^{\alpha_{obs}}m_{obs}(Inside, Z_7)=0.75.$$
$$^{\alpha_{obs}}m_{obs}(Neigh\cup Far, Z_7)=0.$$
$$^{\alpha_{obs}}m_{obs}(\Omega, Z_7)=0.25.$$
$$^{\alpha_{obs}}m_{obs}(Inside, Z_8)=0.5.$$
$$^{\alpha_{obs}}m_{obs}(Neigh\cup Far, Z_8)=0.25.^{\alpha_{obs}}m_{obs}(\Omega, Z_8)=0.25.$$

Hence, conjunctive results are:

$$m_{pre\cap obs}(Inside, Z_7)=0.05$$
$$m_{pre\cap obs}(Inside, Z_8)=0.225$$

$$m_{pre\cap obs}(Inside, Z_7) < m_{pre\cap obs}(Inside, Z_8) \quad (31)$$

With:

$$m_{pre\cap obs}(\phi, Z_7)\simeq 0.71\in Line\,A$$
$$m_{pre\cap obs}(\phi, Z_8)\simeq 0.42\in Line\,A$$

DS normalization leads to:

$$m_{pre\oplus obs}(Inside, Z_7)=0.17$$
$$m_{pre\oplus obs}(Inside, Z_8)=0.39$$

$$m_{pre\oplus obs}(Inside, Z_7) < m_{pre\oplus obs}(Inside, Z_8) \quad (32)$$

With $1-\alpha_{obs}=0.75$, the DS normalization results in (32) are consistent w.r.t (31) and to the scenario.

From this Example1, we can see that if the different $m_{pre\cap obs}(\phi, Z_i)$ belong to different lines (as obtained with $1-\alpha_{obs}=0.95$), DS combination can easily lead to inconsistent location results. To avoid this issue we should get $(m_{pre\cap obs}(\phi), Z_i)\in lineA\ \forall Z_i$ which requires $max((m_{pre\cap obs}(\phi), Z_i))\leqslant 0.75$. The latter is satisfied by taking $1-\alpha_{obs}\leq 0.75$ *i.e.* by discounting the observation with $\alpha_{obs}\geq 0.25$. Nevertheless, if we consider that both observation and prediction are *equally* reliable, we get $(1-\alpha_{obs})\cdot(1-\alpha_{pre})=(1-\alpha)^2\leq(max(m_\phi)=0.75)$ which leads to $\alpha\geq 0.14$. Finally, for a general reasoning, if n sources should be discounted differently, their discounting factors must satisfy $(1-\alpha_1)\cdot\ldots\cdot(1-\alpha_n)\leq(max(m_\phi)=0.75)$ to avoid counter-intuitive results in similar cases of our study.

REFERENCES

[1] Ehsan Ahvar, Nafiseh Daneshgar-Moghaddam, Antonio M. Ortiz, Gyu Myoung Lee, and Noel Crespi. On analyzing user location discovery methods in smart homes: A taxonomy and survey. *Journal of Network and Computer Applications*, 76:75 – 86, 2016.

[2] Jaeseok Yun and Sang-Shin Lee. Human movement detection and identification using pyroelectric infrared sensors. *Sensors*, 14(5):8057–8081, 2014.

[3] P. Zappi, E. Farella, and L. Benini. Tracking motion direction and distance with pyroelectric ir sensors. *IEEE Sensors Journal*, 10(9):1486–1494, Sept 2010.

[4] G. Monaci and A. Pandharipande. Indoor user zoning and tracking in passive infrared sensing systems. In *2012 Proceedings of the 20th European Signal Processing Conference (EUSIPCO)*, pages 1089–1093, Aug 2012.

[5] M. Danancher, J. J. Lesage, L. Litz, and G. Faraut. Online location tracking of a single inhabitant based on a state estimator. In *2013 IEEE Int Conf on Systems, Man, and Cybernetics*, pages 391–396, Oct 2013.

[6] A. L. Ballardini, L. Ferretti, S. Fontana, A. Furlan, and D. G. Sorrenti. An indoor localization system for telehomecare applications. *IEEE Trans on Systems, Man, and Cybernetics: Systems*, 46(10):1445–1455, Oct 2016.

[7] M. P. Fanti, G. Faraut, J. J. Lesage, and M. Roccotelli. An integrated framework for binary sensor placement and

inhabitants location tracking. *IEEE Trans on Systems, Man, and Cybernetics: Systems*, PP(99):1–7, 2016.

[8] B. Yang, Y. Lei, and B. Yan. Distributed multi-human location algorithm using naive bayes classifier for a binary pyroelectric infrared sensor tracking system. *IEEE Sensors Journal*, 16(1):216–223, Jan 2016.

[9] B. Yang and M. Zhang. Credit-based multiple human location for passive binary pyroelectric infrared sensor tracking system: Free from region partition and classifier. *IEEE Sensors Journal*, 17(1):37–45, Jan 2017.

[10] P. M. Djuric, M. Vemula, and M. F. Bugallo. Target tracking by particle filtering in binary sensor networks. *IEEE Transactions on Signal Processing*, 56(6):2229–2238, June 2008.

[11] J. Lu, J. Gong, Q. Hao, and F. Hu. Space encoding based compressive multiple human tracking with distributed binary pyroelectric infrared sensor networks. In *2012 IEEE Int Conf(MFI)*, pages 180–185, Sept 2012.

[12] J. Lu, T. Zhang, Q. Sun, Q. Hao, and F. Hu. Binary compressive tracking. *IEEE Transactions on Aerospace and Electronic Systems*, PP(99):1–1, 2017.

[13] Nisheeth Shrivastava, R Mudumbai U Madhow, and S Suri. Target tracking with binary proximity sensors: fundamental limits, minimal descriptions, and algorithms. In *SenSys*, 2006.

[14] A. Hadj Henni, O. Bennis, R. Ben Bachouch, Y. Parmantier, and N. Ramdani. A multiplex binary pir sensing approach for a telehome-care application. In *2017 IEEE SENSORS*, pages 1–3, Oct 2017.

[15] P.Smets and R. Kennes. The transferable belief model. *Artificial Intelligence*, 66:191234, 1994.

[16] Glenn Shafer. *A Mathematical Theory of Evidence*. Princeton University Press, 1976.

[17] Thierry Denux and Amel Ben Yaghlane. Approximating the combination of belief functions using the fast mbius transform in a coarsened frame. *International Journal of Approximate Reasoning*, 31(1):77 – 101, 2002.

[18] Yi Yang et al. A novel approximation of basic probability assignment based on rank-level fusion. *Chinese Journal of Aeronautics*, 26(4):993 – 999, 2013.

[19] A. Dallil, M. Oussalah, and A. Ouldali. Sensor fusion and target tracking using evidential data association. *IEEE Sensors Journal*, 13(1):285–293, Jan 2013.

[20] A. Martin. Comparative study of information fusion methods for sonar images classification. In *2005 7th Int Conf on Inf Fusion*, volume 2, pages 7 pp.–, July 2005.

[21] Z. Elouedi, K. Mellouli, and P. Smets. Assessing sensor reliability for multisensor data fusion within the transferable belief model. *IEEE Trans on Systems, Man, and Cybernetics, Part B (Cybernetics)*, 34(1):782–787, 2004.

[22] A. Martin, A. L. Jousselme, and C. Osswald. Conflict measure for the discounting operation on belief functions. In *2008 11th Int Conf on Information Fusion*, pages 1–8, June 2008.

[23] Lotfi A. Zadeh. Book review: A mathematical theory of evidence. *AI Magazine*, 5(3):81–83, 1984.

[24] A. Tchamova and J. Dezert. On the behavior of dempster's rule of combination and the foundations of dempster-shafer theory. In *2012 6th IEEE Int Conf Intelligent Systems*, pages 108–113, Sept 2012.

[25] Bo Yang, Jing Luo, and Qi Liu. A novel low-cost and small-size human tracking system with pyroelectric infrared sensor mesh network. *Infrared Physics Technology*, 63:147 – 156, 2014.

[26] A Hadj Henni, D Pasquier, and N Betrouni. A transferable belief model decision support tool over complementary clinical conditions. In *Bioinformatics and Biomedical Engineering, LNCS vol 10814*, pages 409–420, Cham, 2018. Springer.

[27] F. Delmotte and P. Smets. Target identification based on the transferable belief model interpretation of dempster-shafer model. *IEEE Trans on Systems, Man, and Cybernetics - Part A: Syst and Humans*, 34(4):457–471, 2004.

[28] E. Ramasso, M. Rombaut, and D. Pellerin. State filtering and change detection using tbm conflict application to human action recognition in athletics videos. *IEEE Trans on Circuits and Systems for Video Technology*, 17(7):944–949, July 2007.